Microcellular epoxy/graphene nanocomposites with outstanding electromagnetic interference shielding and mechanical performance by overcoming nanofiller loading/dispersion dichotomy

Xun Fan, Qiang Gao, Yusong Gao, Geyang Zhang, Fei Huang, Ronglin Xiao, Wei Liu, Fengchao Wang, Jianbin Qin, Emiliano Bilotti, Han Zhang, Xuetao Shi, Guangcheng Zhang

PII: S0266-3538(21)00356-0

DOI: https://doi.org/10.1016/j.compscitech.2021.109000

Reference: CSTE 109000

To appear in: *Composites Science and Technology*

Received Date: 11 March 2021

Revised Date: 28 July 2021

Accepted Date: 14 August 2021

Please cite this article as: Fan X, Gao Q, Gao Y, Zhang G, Huang F, Xiao R, Liu W, Wang F, Qin J, Bilotti E, Zhang H, Shi X, Zhang G, Microcellular epoxy/graphene nanocomposites with outstanding electromagnetic interference shielding and mechanical performance by overcoming nanofiller loading/dispersion dichotomy, *Composites Science and Technology*, https://doi.org/10.1016/j.compscitech.2021.109000.

Author Statement

Xun Fan, Xuetao Shi and Guangcheng Zhang designed the experiments. Xun Fan, Qiang Gao and Yusong Gao developed the strategy. Xun Fan, Yusong Gao and Geyang Zhang prepared GA, m-EP/rGO solids and m-EP/rGO foams. Xun Fan, Fei Huang and Ronglin Xiao performed the SEM, TEM, AFM, XPS, TGA, DSC and XRD tests and analyzed related data. Xun Fan, Wei Liu, Fengchao Wang and Jianbin Qin performed thermal conductivity, electrical conductivity, EMI SE and compressive property tests and analyzed related data. Xun Fan, Xuetao Shi, Guangcheng Zhang, Emiliano Bilotti and Han Zhang interpreted discussed the results. Xun Fan analyzed the data and wrote the paper. Xun Fan, Xuetao Shi and Han Zhang revised the paper and responded the reviewers.

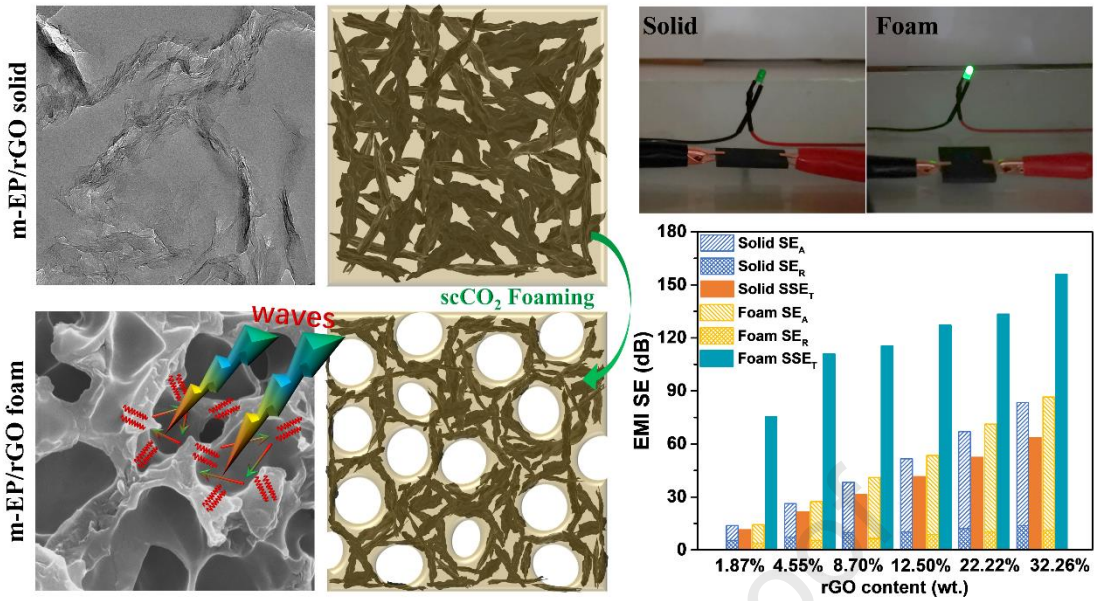

Microcellular epoxy/graphene nanocomposites with outstanding electromagnetic interference shielding and mechanical performance by overcoming nanofiller loading/dispersion dichotomy

Xun Fan[a], Qiang Gao[a], Yusong Gao[b], Geyang Zhang[b], Fei Huang[c], Ronglin Xiao[c], Wei Liu[a], Fengchao Wang[b], Jianbin Qin[a], Emiliano Bilotti[b,d], Han Zhang[b,d], Xuetao Shi[a]**, Guangcheng Zhang[a]*

[a]Shaanxi Key Laboratory of Macromolecular Science and Technology, School of Chemistry and Chemical Engineering, Northwestern Polytechnical University, Xi'an, Shaanxi 710072, P. R. China

[b]NPU-QMUL Joint Research Institute of Advanced Materials and Structures, Northwestern Polytechnical University, Xi'an, 710072, PR China

[c]Shaanxi Coal Chemical Industry Technology Research Institute Co. Ltd, Xi'an, Shaanxi 710070, P. R. China

[d]School of Engineering and Materials Science, Queen Mary University of London, Mile End Road, E1 4NS London, United Kingdom

*Corresponding author. Tel.: +86-29-88431672

E-mails: zhangguc@nwpu.edu.cn (G. Zhang)

shixuetao@nwpu.edu.cn (X. Shi)

Abstract

With the rapid evolvement of wireless communication technologies, the ever increasing needs to prevent electromagnetic waves (EMWs) pollutions have urged the development of lightweight materials with excellent electromagnetic interference (EMI) shielding property. However, achieving desired EMI shielding performance often requires high loadings of conductive nanofillers, like graphene, which poses challenges to control the nanoparticle dispersion and the mechanical performance of the nanocomposite. Herein, we demonstrate a method to fabricate highly-loaded (>30 wt.%) graphene in microcellular epoxy nanocomposites, successfully overcoming the long-lasting dichotomy in the field of nanocomposites of high filler loading and dispersion. By utilizing supercritical CO_2 foaming method, modified thermosetting epoxy-based

nanocomposite was foamed with multiple interfaces and tunable microcellular cells. In addition, a rearrangement of nanofillers during foaming process is favorable for more intense conductive network, leading to enhanced EMWs attenuation by repeated reflections and absorptions. An optimal combination of electrical conductivity (314 $S \cdot m^{-1}$), EMI shielding effectiveness (86.6 dB and 156.3 $dB/(g/cm^3)$), compressive strength (27.4 MPa) and density (0.55 $g \cdot cm^{-3}$) has been achieved for foamed nanocomposite with 32.26 wt. % graphene content. This versatile method opens up an easy route to fabricate lightweight structural foams with high nanofiller contents, which could be used in many applications such as electronics, robotics, and aircrafts.

Key words: Graphene; Epoxy foam; High nanofiller loading; Microcellular nanocomposites; Electromagnetic interference shielding effectiveness

1. Introduction

With the rapid evolvement of the information and communication technology, especially the use of 5G technology, electronic devices have become an integral part of our society with the capability of high-speed data transmission and portability. However, the increased usage of these electronic devices and other equipment also raises concerns on potential electromagnetic radiation and electromagnetic waves (EMWs) pollution, limiting the rapid pace of development for many technologies and applications. Clearly, novel materials and structures with high electromagnetic wave shielding and absorption capabilities are of great necessity to provide high safety assurance for next-generation electronic devices. Additional features like lightweight and high mechanical performance are also highly desired for their uses in portable electronics, healthcare devices, as well as transport sectors like aerospace or automotive [1-4].

Several governing factors, such as electrical conductivity, magnetic permeability and internal structural design, should be considered to achieve high electromagnetic interference (EMI) shielding performance [5]. As evidenced by the famous Faraday cage in 1836, high electrical conductivity is essential to provide the good shielding to block the EMWs, hence many traditional EMI shielding materials are made out of metals [6-8]. However, the high density and poor corrosion resistance of metallic materials often limit their utilization where the lightweight and portable features are required. To overcome these challenges and fulfill evolving demands and requirements, conductive polymer composites (CPCs) have been extensively explored in recent

years to provide both high EMI shielding efficiency and lightweight structural properties. Considering the wide range of options on conductive fillers, especially nanofillers with high electrical conductivity and permittivity, like carbon nanotubes and graphene nanoplatelets, together with ease of processing from various polymer matrices, high electrical conductivity can be achieved in CPCs for high EMI shielding effectiveness (SE). For instance, Liang et al. used solution mixing to fabricate the epoxy/graphene CPC with 15 wt.% graphene content, exhibiting EMI SE of about 21 dB at 8.2-12.4 GHz (X-band) [9]. Similarly, Ling et al. prepared polyetherimide/graphene composite with 10 wt.% of reduced graphene oxide (rGO), and obtained an EMI SE of 20.0 dB at X-band [10]. The higher graphene loading (20.0 wt.%) in polyvinyl chloride/graphene composite by solution mixing method exhibited an EMI SE of 29.5 dB at X-band [11].

It is well acknowledged that the high loading of nanofillers could lead to severe agglomeration due to the extremely large surface areas of nanofillers, posing great challenges in the processing of CPCs. To overcome the potential aggregation of nanofillers in polymer matrix and to avoid consequent effects on conductive network and properties of processability and mechanical stress, constructing 3D framework of carbon-based fillers such as graphene aerogel has also been explored recently as a new strategy [12]. Chen *et al*. have prepared poly(dimethyl siloxane)/graphene foam, with less than 0.8 wt. % graphene loading and EMI SE of 30 dB at X-band [13]. Furthermore, Chen *et al*. reported an outstanding conductivity of 148 S m^{-1} and EMI SE of ~33 dB at X-band for the epoxy nanocomposite with 0.66 wt.% CNT sponge, which is higher than conventional epoxy nanocomposites with 20 wt. % CNTs [14]. Huangfu *et al.* reported a remarkable EMI SE of 35 dB at the X-band for epoxy/reduced graphene oxide (rGO)/Fe_3O_4 nanocomposites prepared by the epoxy infiltration into graphene aerogel functionalized with Fe_3O_4 (1.5/1.2 wt.% of Fe_3O_4/rGO) [15]. In addition, Yan et al. prepared the polystyrene composite with 3.47 vol. % 3D segregated rGO, representing a higher EMI SE of 45.1 dB at X-band [16]. Although many promising results can be found from the literatures, challenges remain on how to further increase the conductive nanofillers loading for enhanced EMI SE values, as the loading level is restricted by the graphene aerogel structure.

Apart from increasing the intrinsic materials properties, such as electrical conductivity, an equally important and effective route to achieve high EMI SE is by controlling the internal structure of shielding mateirals. As indicated from graphene aerogel structure, a porous structure

consisting of multiple interfaces can effectively reflect the EMWs within the materials, leading to a high EMI shielding efficiency due to the waves attenuation during multi reflections [17]. Apparently, preparing conductive composite foams with microcellular structures are one of the great strategies to achieve these targets. Thanks to the strong extensional flow during cell growth and the consequent enrichment and rearrangement of conductive fillers, a more intense electrical conductive network in foamed composites is promoted. Zhang *et al.* have reported the graphene redistribution on cell walls in microcellular polymethylmethacrylate/graphene nanocomposites, resulting in a denser conductive network, higher electrical conductivity, as well as better EMI shielding performance [18]. Hamidinejad *et al.* reported a microcellular CPCs consisting of polyethylene/graphene nanoplatelets, with reduced percolation thresholds (9.8 vol.% nanofiller of foamed sample vs. 19 vol.% of solid sample) and high EMI SE of 31.6 dB at X-band [19]. Shen *et al.* have prepared a lightweight polyurethane/graphene nanocomposite with 3D network graphene prepared by dip-coating method and demonstrated a high EMI SE of 57.7 dB at X-band [20]. However, it is worth noting that these aerogel-based nanocomposites and foamed nanocomposites structures are often associated to mechanical brittleness, limiting their development in lightweight structural applications.

In this study, these two-long lasting dichotomies in the field of nanocomposites are explored, namely the challenge of balancing high nanofiller loadings and nanofiller dispersion levels, as well as the challenge of achieving high electrical/electromagnetic properties while preserving mechanical performance in porous foam structures. A facile fabrication method to produce highly loaded yet well dispersed modified epoxy/graphene nanocomposites with tunable microcellular structures has been developed, based on a significantly enhanced foamability of modified thermosetting resins. Thus, this work provides a new direction of designing and fabricating nanocomposites with tailored internal structures and desired properties, for applications ranging from portable electronics to healthcare devices.

2. Materials and methods

2.1 Materials

Epoxy resin (Diglycidyl ether of bisphenol-A, Mw: 1428～2000 g/mol) and hyperbranched epoxy resin (E102, Mw: 3200～3600 g/mol) were purchased from Yueyang petrochemical Co., Ltd., and Wuhan Hyperbranched Polymer Resin Science & Technology Co., Ltd., China, respectively. 2-ethyl-4-methylimidazole (2E4MZ, 96%), 3-glycidyloxypropyltrimethoxysilane

(KH560, 97%) and graphite (>99.99%) were bought from Aladdin industrial Co., Ltd., China. Polyether amine (M2070, Mw: 2000 g/mol) was obtained from Huntsman Co., Ltd., U.S.A. and carbon dioxide (CO_2, 99.99%) was from ChangTe gas Co., Ltd., China. The concentrated sulfuric acid (H_2SO_4, 95-98%), sodium nitrate ($NaNO_3$, >99.9%), dichloromethane (CH_2Cl_2), potassium permanganate ($KMnO_4$), hydrazine hydrate (N_2H_4, 80%), hydrogen peroxide (H_2O_2, 30%) and other chemicals were achieved from Sinopharm Chemical Reagent Co., Ltd, China.

2.2 Preparation of modified-epoxy (m-EP)/graphene nanocomposites

Graphene aerogel (GA) was obtained from graphene oxide (GO) that was produced by modified Hummers method (S1, supporting information) as shown in Figure 1a. The GO suspension was reduced by hydrazine hydrate (N_2H_4) (Figure 1b). 5 g GO was dispersed in 1000 ml deionized water and stirred for 12 h, followed by the addition of 50 ml N_2H_4 (24 wt.%) and mixing for 30 min. As shown in Figures 1a and 1b, the beaker with prepared GO dispersion was placed in oven at 90℃ for 3 days to obtain reduced graphene (rGO) hydrogel block that was then turned into porous GA by freeze drying. Epoxy resin, hardener, hyperbranched epoxy (E102, Figure S2) and prepared plasticizer (KM, S2, supporting information, Figure S1) were dissolved in dichloromethane (CH_2Cl_2). The epoxy and hardener were added with 20:1 weight ratio. The epoxy/E102/KM mixing solution with 90:10:5 of epoxy with hardener added, E102 and KM weight ratio was dried at 35 ℃ to fully remove the solvent and was turned into powder. The following curing reaction of epoxy/E102/KM (m-EP) was carried out inside the mold under 30 MPa at 120 ℃ for 2 hours. The addition of E102 and KM into the epoxy matrix was to improve the molecular flexibility to enhance its foamability [21, 22]. The solid m-EP was prepared as reference sample.

The introduction of rGO into m-EP matrix was achieved by the vacuum-assisted infiltration firstly (Figure 1c). The nanofiller concentration was controlled by different uncured m-EP concentrations in m-EP/CH_2Cl_2 solution. In detailed process, porous GA was infiltrated by m-EP/CH_2Cl_2 solution, then the uncured m-EP was wrapped on graphene surface after removing solvent at 35℃. Subsequently, the uncured m-EP/rGO composites was grinded into powder and then placed into chamber to prepare m-EP/rGO nanocomposites by thermal compression with the processing conditions of 30MPa/2h/120℃ (Figure 1d and 1e). A series of prepared m-EP/rGO nanocomposites with different ratio between m-EP and rGO were recorded in Table S1. The m-EP/rGO nanocomposites with different rGO loadings were marked as following: 0 wt.% (m-EP),

1.87 wt.% (m-EP/rGO-1.87), 4.55 wt.% (m-EP/rGO-4.55), 8.70 wt.% (m-EP/rGO-8.70), 12.50 wt.% (m-EP/rGO-12.50), 22.22 wt.% (m-EP/rGO-22.22) and 32.26 wt.% (m-EP/rGO-32.26) rGO, respectively. These samples were prepared with thickness of 2 mm in the mold by a post curing process with gradient temperature program of 120℃/2h, 140℃/2h and 160℃/2h.

2.3 Preparation of microcellular m-EP/graphene nanocomposites

m-EP/rGO nanocomposites were foamed by applying the supercritical CO_2 ($scCO_2$), in which CO_2 was pumped into micro-autoclave (Anhui Kemi Machinery Technology Co., Ltd., China) through supercritical fluid pump (S10SNXP1, SSI, U.S.A.). The real-time temperature was controlled and monitored by an automatic temperature control unit (Xiamen Yudian Automation Technology Co., Ltd., China). The saturated condition of 25MPa/50℃/48h was used to maintain the temperature and pressure during the foaming process to ensure the materials has achieved a saturated CO_2 absorption. Afterwards, all gases were released during 10s and the CO_2 saturated samples were placed in an oil bath to proceed with the free foaming process under 3～60s foaming time and 120℃ foaming temperature. The foamed samples were immersed in the ice water bath to stabilize their cellular macrostructures, followed by storing under -5℃ for another two weeks to fully release any residual CO_2 before the characterization.

2.4 Characterizations

Both GO and rGO were examined by X-ray photoelectron spectroscopy (XPS, Kratos Axis Ultra DLD, U.K.) equipped with scanning monochromatic Al-Ka energy source (hv=1486.6 eV) and Raman spectroscopy (Alpha300R, WITec, Germany) using 532 nm wavelength laser. X-ray diffraction pattern (XRD, SHIMADZU, Japan) with Cu Kα radiation (λ=0.15418 nm) was used to measure crystalline structure of GO, rGO and m-EP/rGO nanocomposites from 5° to 80° at 5°/min scanning speed. The nuclear magnetic resonance (NMR, Bruker Avance DRX 400, U.S.A.) was used to analyze molecular structure (Figrue S2) of hyperbranched epoxy (E102) at 400 MHz with $CDCl_3$ as solvent. Thermogravimetric analysis (TGA, TA Q50, U.S.A.) was carried out from 50 ℃ to 800℃ at 10℃/min under nitrogen atmosphere. Transmission electron microscope (TEM, FEI-Talos F200x, U.S.A.) and atomic force microscope (AFM, Dimension, Bruker, Germany) were employed to characterize the morphology of GO and rGO. The fracture surfaces of m-EP/rGO solids and foams were examined by field emission scanning electron microscopy (FESEM, FEI Verios G4, U.S.A.) and scanning electron microscopy (SEM, VEGA 3 LMH, Czech). The electrical conductivity was measured by a four-point probe resistivity measurement

system (RTS-9). Besides, nanoindentation test (Hysitron-TI980, U.S.A.), compression measurement (SANS CMT5105, China), statistic of cell parameters using Pro-plus software, density and volume expansion ratio calculation, and thermal conductivity (Hot Disk instrument, AB Corporation, Sweden) were investigated and presented in materials and methods (S3-S7, Supporting information). EMI SE of specimens was achieved by dealing with scattering parameters (S_{11}, S_{12}, S_{22} and S_{21}) measured by vector network analyzer (VNA, Agilent N5230, USA) in X-band (8.2-12.4 GHz) (S8, supporting information).

3. Results and discussion

3.1 Characterization of microcellular m-EP/rGO nanocomposites

Figure 1 presents the overall fabrication process of the microcellular modified-epoxy/E102/KM/graphene (m-EP/rGO) nanocomposites with their resulted morphologies. As shown in Figure 1a and 1b, the graphene oxide (GO) suspension was reduced by hydrazine hydrate (N_2H_4) to fabricate reduced graphene oxide (rGO) hydrogel, which was then lyophilized, leading to the formation of porous graphene aerogel (GA) [23]. The diluted m-EP resin was then infiltrated into GA assisted by vacuum-assisted infiltration (Figure 1c). During the thermal compression process (Figure 1d and 1e), the as-prepared uncured m-EP/rGO architecture was powdered and compressed into m-EP/rGO nanocomposites by simultaneously crosslinking reaction with dense graphene interconnections.

Subsequently, the supercritical CO_2 ($scCO_2$) foaming process was utilized on the cured nanocomposites (Figure 1f), introducing microporous cells with graphene redistributed and enriched in the cell walls. Figure 1g shows the morphologies of GA as well as fabricated microcellular m-EP/rGO nanocomposites, confirming the well-controlled cell size distribution with highly concentrated yet well dispersed graphene nanoplatelets within the cell walls, which are essential for mechanical and electrical properties. The tailored m-EP structure (Figure 3) also successfully enabled the foaming process of crosslinked m-EP/rGO nanocomposites, overcoming another dichotomy between the thermosetting epoxy and the microcellular foamability.

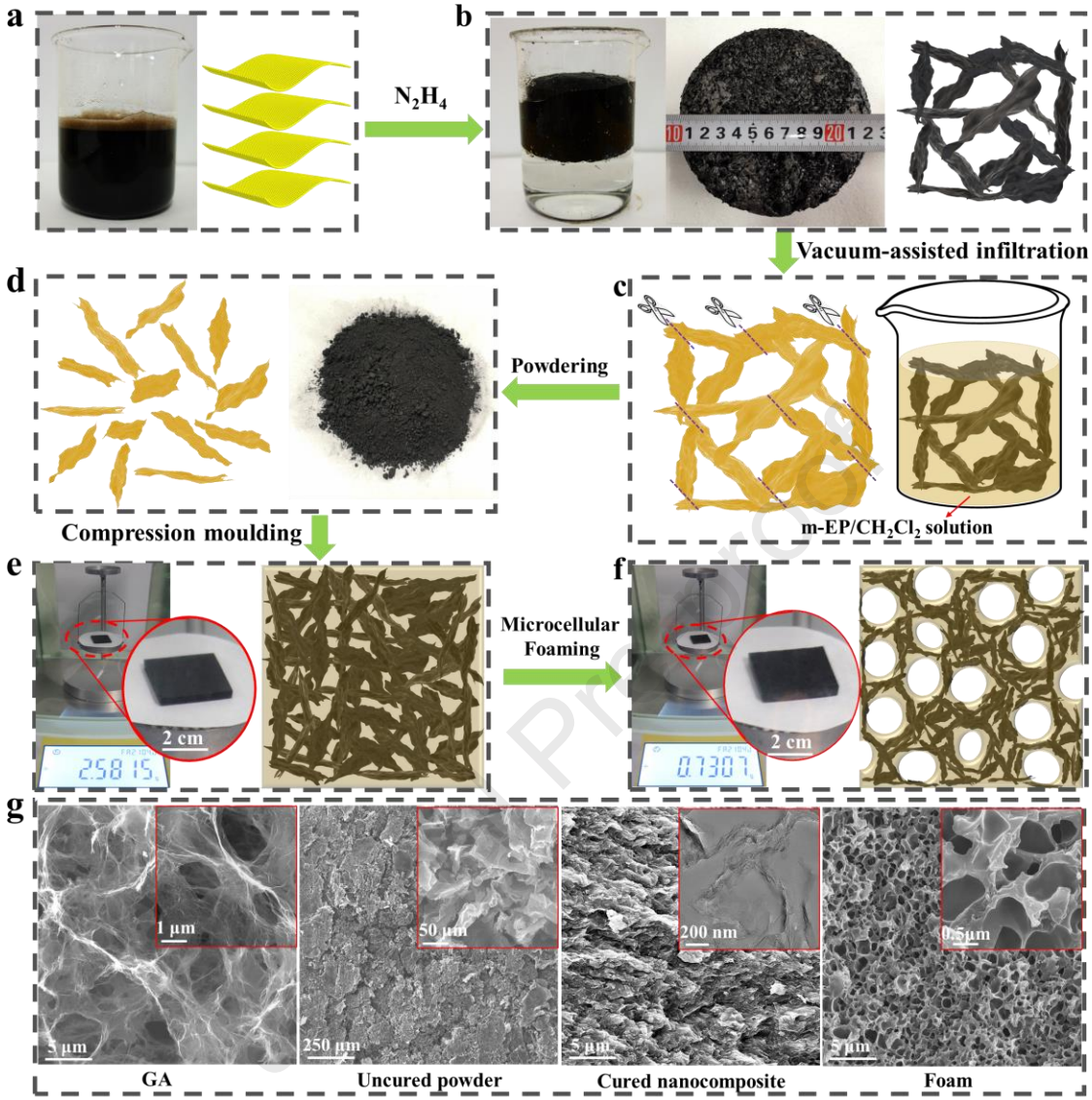

Figure 1 The schematic illustrations of the fabrication process of microcellular modified-epoxy/E102/KM/graphene (m-EP/rGO) nanocomposites: (a) graphene oxide (GO) suspension with 5 mg/ml concentration; (b) reduced graphene oxide (rGO) hydrogel (left), aerogel (GA, middle) and schematic graphene 3D framework (right); (c) vacuum-assisted infiltration of m-EP resin into GA with uncured m-EP wrapped on surface of GA after evaporation of organic solvents; (d) grinding to obtain the uncured m-EP/rGO in powder form for subsequent curing under compression moulding; (e) cured m-EP/rGO nanocomposite with dense rGO distribution; (f) introduce porous structure into m-EP/rGO nanocomposite by supercritical CO_2 ($scCO_2$) foaming method; (e) SEM images showing graphene morphologies and distributions in different

microstructures of GA, uncured m-EP/rGO, cured nanocomposite and microcellular m-EP/rGO nanocomposite (foaming time: 20 s and foaming temperature: 120 ℃)

3.2 Morphology and interaction between graphene and m-EP matrix

Clearly, both dispersion of nanofillers and the interaction between nanofillers and matrix are essential in achieving desired performance of nanocomposites. During the preparation of m-EP/rGO nanocomposites by resin infiltration into GA, the effective interfacial interaction between graphene flakes and the m-EP matrix is crucial for the further powdering and curing under compression moulding. As shown in Figure 2a, epoxide and carboxyl groups on GO nanofiller react with N_2H_4, with C=C and C=N bonds as reaction products [24-26]. According to the TGA analysis, there are still about 9.87 wt.% of oxide groups on rGO surface, indicating a certain amount of hydroxyl group remained on rGO that could facilitate the interaction between rGO and m-EP resin. This has been confirmed by the X-ray photoelectron spectroscopy (XPS, Figure 2c and Figure S3) spectra, demonstrating that characteristic C 1s and O 1s peaks and the content of C and O element changed from GO to rGO, with the C/O ratio increased from 1.67 to 7.89, which is in agreement with the previously reported results [25]. The interactions between m-EP and rGO can be attributed to both the covalent bonding caused by crosslinked reaction and non-covalent bonding including hydrogen bonding and π-π stacking, which are related to polar groups and aromatic rings, respectively [27, 28].

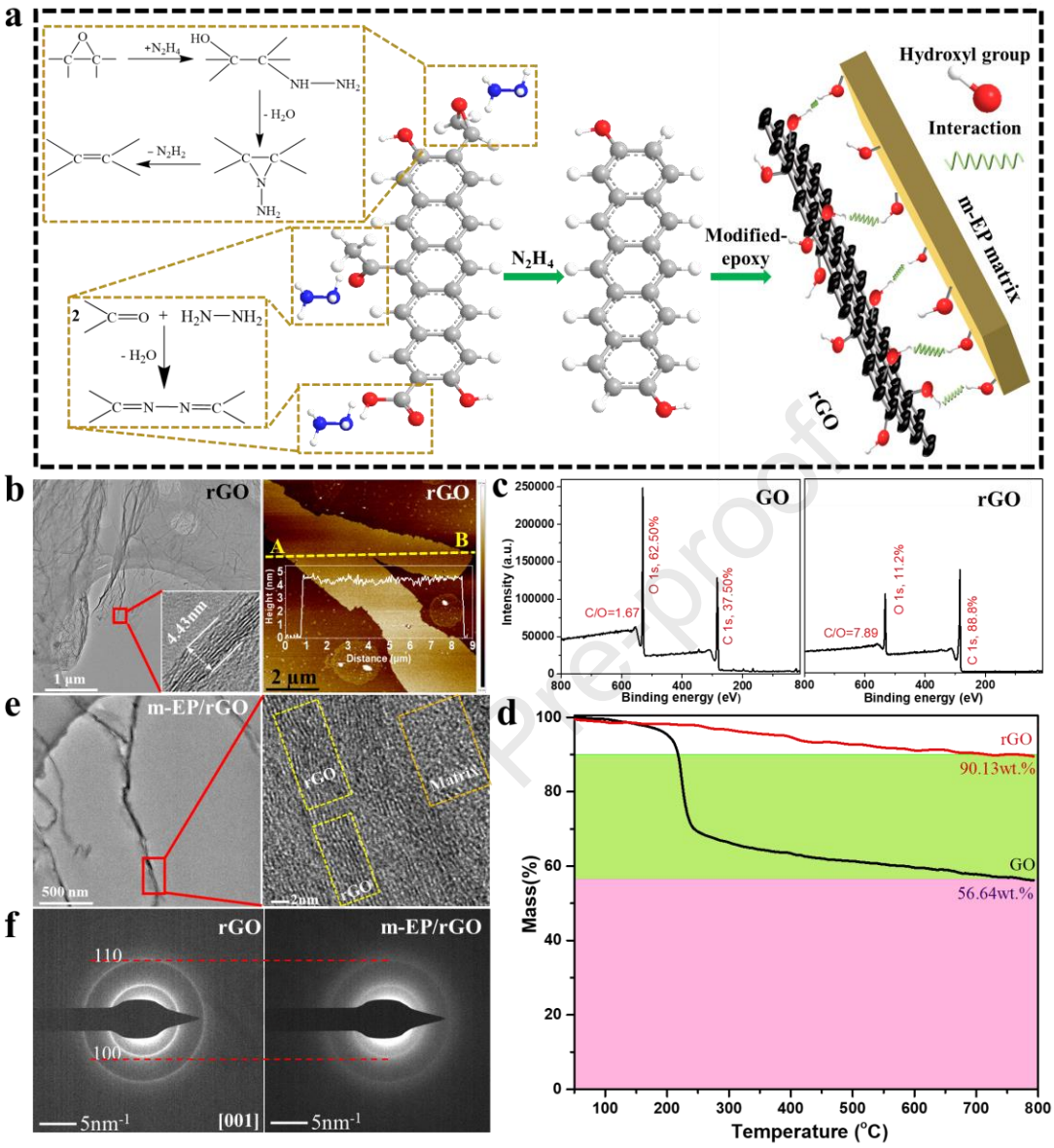

Figure 2 Characterization of interfacial interaction between rGO and m-EP matrix: (a) schematic presenting the reaction of epoxide and carboxyl groups of rGO and hydrazine hydrate (N_2H_4), as well as the existing hydroxide groups on rGO surface interacting with matrix; (b) transmission electron microscopy (TEM) and atomic force microscopy (AFM) microphotographs of rGO (insets shows high resolution TEM (HRTEM) image and thickness distribution of rGO); (c) X-ray photoelectron spectroscopy (XPS) widen scanning with the ratios of C and O elements in GO and rGO; (d) thermogravimetric analysis (TGA) measuring weight loss of GO and rGO after heating to 800 ℃ in N_2 atmosphere; (e) TEM images of graphene in cured m-EP/rGO nanocomposite and

related HRTEM image (rGO content is 4.55 wt.%); (f) selected-area electron diffraction (SAED) maps of rGO and cured nanocomposite with 4.55 wt.% rGO

Figure 2b shows the morphology of rGO with wrinkles and folds observed, and a typical flake thickness of 4.43 nm (about 13 layers) measured by transmission electron microscopy (TEM) and atomic force microscopy (AFM), confirming the influence of reduction process on rGO structure (GO morphology can be found in Figure S4). The results of field emission electron scanning microscopy (FESEM), X-ray diffraction (XRD) patterns and Ramon spectra in Figures S5-S7 illustrate the features of GA and confirm restoration of conjugation sp^2 regions and π-π stacking interaction during reducing GO to rGO [29]. Clearly, the successfully fabricated GA composed of rGO that possesses 4.43 nm thickness and reactive oxide groups benefits for the strong interaction between rGO and m-EP resins and then effective formation of electrical conductive network in m-EP/rGO nanocomposites. The porous structure of aerogel also acts as a stable scaffold to facilitate the epoxy infiltration process without affecting the nanoparticle agglomeration due to sufficient contact surface area and reactive groups. Figure 2e presents rGO dispersion in m-EP/rGO nanocomposite, with the observed nanoscale thickness of dispersed graphene flakes. The high resolution TEM (HRTEM) also reveals no obvious crack or delamination in m-EP/rGO interfacial regions, further confirming the good interaction between nanofillers and matrix. The diffraction rings in selected-area electron diffraction (SAED) of Figure 2f represent that typical [100] and [110] lattice planes in m-EP/rGO are less sharp, on contrast to the clear rings from pure rGO, due to the presence of amorphous carbon structure from m-EP. The amorphous carbon structure of m-EP weakens the intensities of electron diffraction, which indicates graphene flake was wrapped by m-EP matrix with strong interaction [30]. Furthermore, a series of m-EP/rGO nanocomposites (rGO contents ranging from 1.87 to 32.26 wt.%) were successfully prepared with homogeneous nanofiller dispersion.

3.3 Tuning the foamability of thermosetting resins with modified epoxy

As mentioned earlier, microcellular structure can render multi-reflection and attenuation of EMWs, hence greatly enhance the EMI SE of materials [18, 19]. However, it is worth noting that most of the literature has been focused on thermoplastic microcellular foams, such as polyethylene, polypropylene, polystyrene, polymethylmethacrylate and polylactic acid [31]. Despite the excellent mechanical properties, chemical and thermal resistance, thermosetting microcellular foams, like epoxy foams depending on $scCO_2$ foaming method, are rarely reported due to their

heavily chemical cross-linked networks, which are unfavorable for the mass transmission of blowing gases [32].

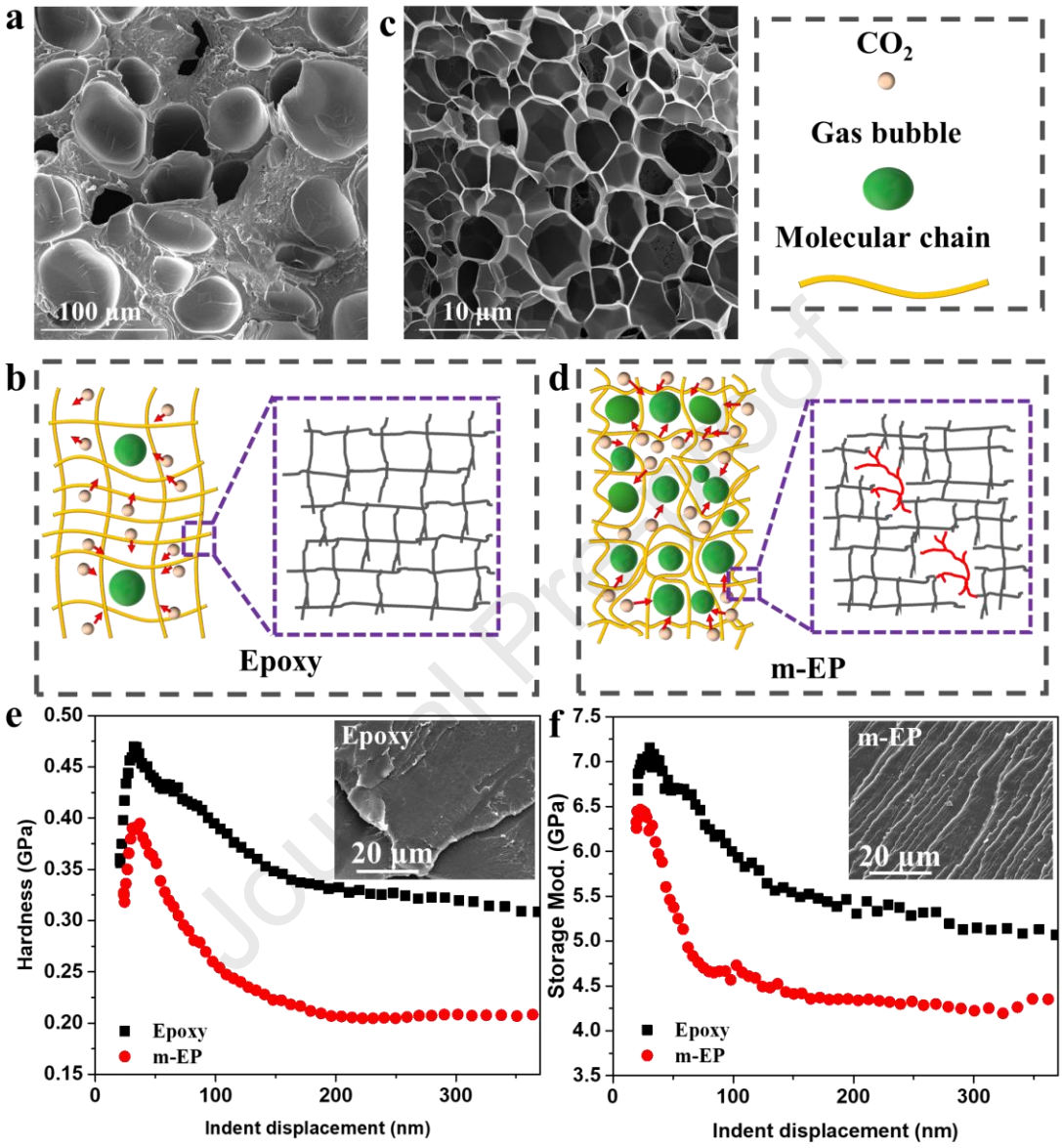

Figure 3 Foamability of neat epoxy and epoxy/E102/KM (m-EP) matrices: (a) microstructure of fracture surface of neat epoxy foam and (c) m-EP foam at 20 s foaming time and 120 ℃ foaming temperature; schematic diagram illustrating CO_2 transferring and foaming process in (b) epoxy and (d) m-EP matrix; the measured hardness (e) and storage modulus (f) from nano dynamic mechanical analysis for neat epoxy and m-EP system (inserts present the surface morphologies of epoxy and m-EP matrices)

Clearly, overcoming the challenge of the epoxy foamability could also open up a brand-new avenue of cellular nanocomposites for EMI applications with many existing advantages of thermosetting resins. Thus, modification of epoxy resins has been performed in this work with organic precursor (KM, Figure S1) as well as the hyperbranched epoxy (E102, Figure S2), enabling the subsequent foaming process by $scCO_2$. The foaming capability of neat epoxy resins was examined by applying $scCO_2$ foaming method. As expected, irregular and non-uniform cell morphologies can be found (Figure 3a) due to its high crosslink density which constrains the forming process as illustrated in Figure 3b. On the contrast, with the incorporation of plasticizer (KM) and hyperbranched epoxy (E102) to modify the epoxy matrix (m-EP matrix, Figure 3c and 3d), the gas absorption as well as the subsequent bubble nucleation and growth during foaming process were successfully improved, leading to a relatively homogeneous cell morphology with cell size 1.21 μm and cell density 3.02×10^{11} cells/cm^3, together with an ultra-low foam density (<0.1 g/cm^3, Figure S12). As shown in Figure S8, the combined effects of the E102 where the hyperbranched structure can react with curing agent to form an irregular crosslinked structure, and the KM where the dangling primary amine and soft segment can open epoxide ring and participate in curing reaction to allow molecular movements on m-EP matrix foamability contribute to the obtained microcellular structures with well controlled morphologies [33, 34]. The influence of foaming conditions as well as the ratios of E102 and KM on the cell morphology were discussed and shown in Figures S9-S12. After comparison of cell density and volume expansion ratio of neat epoxy and the prepared m-EP composites in Table S2, the optimized ratio of epoxy to KM and E102 were fixed to be 90:10:5. The mechanical properties (Figure 3e and 3f) are employed to characterize and compare neat epoxy resin and m-EP. Both the storage modulus and hardness were reduced after modifying the epoxy resins that reveal lower glass transition temperature (T_g, Figure S9b), which all facilitated the mobility of polymer chains with correct matrix viscoelasticity upon foaming process [35-37]. Besides, it should note that the neat epoxy matrix applied in previous reported works showed lower density and limited foamability due to restricted polymer chain movability in crosslinked network that enable larger cell size, lower cell density and thicker wall thickness [32, 38, 39].

3.4 High graphene loading in m-EP/rGO nanocomposites with microcellular structures

Thanks to the excellent aforementioned graphene/matrix interaction and relatively homogeneous graphene dispersion, the enhanced foaming capability of m-EP was successfully

transferred into the fabricated m-EP/rGO nanocomposites with a wide range of filler loadings (1.87～32.26 wt.%) without obvious agglomerations even at over 30 wt.% rGO contents. Figures 4b and c, and S13b and c revealed the microstructure of m-EP/rGO nanocomposites before and after the foaming process with different nanofiller loadings. When the rGO loadings were relatively low (1.87 wt.% to 8.70 wt.%), the cell morphologies were not very homogenous with varied unit cell sizes as indicated from the large error bars in Figure 4f. Interestingly, with the increased amount of rGO contents, a more homogeneous cell distribution with small unit size hence a higher cell density was achieved. This is attributed to synergistic effect of the high loading of well dispersed graphene fillers acting as cell nucleating sites and constraining the cell growth during the foaming process. As shown in Figures 4c and f, and S13c, S14 and S15, a clear trend of decreased cell size can be observed with increased amount of rGO, together with a more uniform cell distribution and thinner cell wall. This could be attributed to the increased barrier performance, leading to a synergetic effect between microcellular structure and nanofiller distribution. On the one hand, high loading of well dispersed rGO has led to an increased number of m-EP-rGO interfaces, acting as gas reservoir sites of CO_2 hence more cell nucleating sites (Figure S21), where critical nucleation energy is lowered and heterogeneous bubble nucleation is induced during foaming processes [35]. On the other hand, the re-arrangement of rGO network has also been enabled by the foaming process, leading to an effectively more enriched conductive network within the cell walls as illustrated in Figure 4d, 4d' and 4h. As expected, the electrical conductivity was increased after foaming process, for instance, from 10^{-2} S/m to 10^{-1} S/m at same rGO loading of 4.55 wt.%. The increased electrical conductivity can be visualized from Figure 4e, with the LED bulb under same voltage shown a much brighter light when connected through the foam specimen than solid specimen, confirming the higher amount of electrons passing through the specimen. This is attributed to the enriched rGO network within the cell wall due to stretching and squeezing effects during cell growth, leading to a more effective interconnection of rGO (Figures S16 and S17) [40].

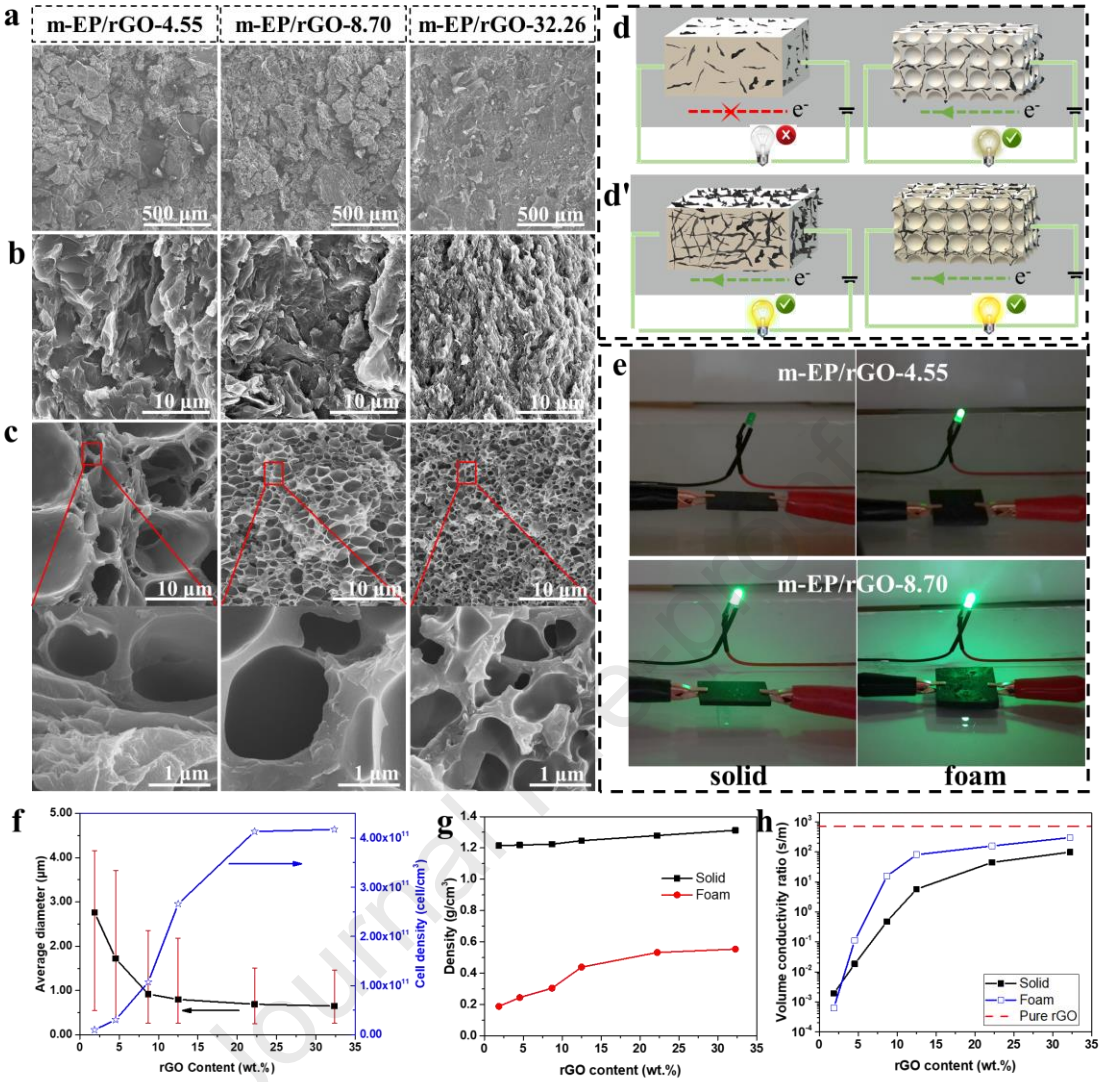

Figure 4 Morphologies and electrical conductivity of m-EP/rGO specimens with various rGO loadings: (a) uncured and (b) solid m-EP/rGO nanocomposites before foaming processes; (c) microcellular m-EP/rGO nanocomposites with different magnifications; (d and d') illustrations of graphene network re-distributions induced by the $scCO_2$ foaming process and (e) indication of electrical performance by connecting the light bulb with solids and foams; (f) average cell diameter and cell density, showing a clear trend of more homogeneous cell distribution and higher cell density with increased amount of rGO contents (the average cell size decreased from 2.77 μm to 0.64 μm, whereas the cell density increased from 9.61×10^{9} cells/cm^3 to 4.19×10^{11} cells/cm^3); (g) density (from 0.18 g/cm^3 to 0.55 g/cm^3) and (h) electrical conductivity of both solid and foam specimens, confirming the lightweight and high electrical conductivity after foaming processes

With the highest nanofiller loading studied in this work (32.26 wt.%), electrical conductivity (3.14×10^2 S/m) of m-EP/rGO foams was achieved (Figure S18), together with uniform cell size and low density of 0.55 g/cm^3 (Figure 4g). No obvious nanofiller agglomeration of nanocomposite was found at such high loading thanks to the strong interfacial interaction between rGO and m-EP. Higher nanofiller content was obtained in m-EP/rGO nanocomposites by vacuum-assisted infiltration method with followed compression moulding, compared to GA-based nanocomposites fabricated via conventional methods with only about 1.0 wt.% graphene loadings [41, 42]. The results of TGA and XRD (Figures S19 and S20) have also confirmed the thermo-stability and rGO contents in all samples, as well as influence of rGO on the nanocomposites' crystallinity [43]. The increased peak shift of XRD patterns caused by the risen proportion of oriented hexagonal carbon of rGO in m-EP/rGO systems confirms the intact structure within the nanocomposites. Therefore, a synergistic effect between high rGO loadings and foaming process of m-EP/rGO has enabled nanocomposite foam a well-controlled cell distribution and low density together with excellent electrical conductivity and homogeneous filler dispersions, successfully solving the long-lasting dichotomy of high loading and homogenous dispersion of nanocomposites. All of these elements are essential in achieving a lightweight structural conductive polymer composite with not only high EMI performance but also preserved mechanical properties.

3.5 Excellent EMI performance with preserved mechanical properties

The electromagnetic shielding efficiency as well as thermal and mechanical properties have been characterized and analyzed systematically for the m-EP/rGO nanocomposites. The expansion in specimen dimensions during the supercritical CO_2 foaming process has led to an increase in thickness as well as the enrichment of electrical conductive nanofiller within the cell walls, benefitting the electromagnetic interference (EMI) shielding effectiveness (SE). Hence, excellent EMI SE performance can be found in current nanocomposites for both solid and foam specimens, especially for foamed those with high rGO loadings, with the absolute SE_T of 83.5 dB and 86.6 dB in the m-EP/rGO-32.26 solid and foam, indicating over 99.999999% shielding efficiency [44]. As shown in Figures 5a, 5a' and 5a", the EMI SE values of m-EP/rGO nanocomposites at X-band (8.2-12.4 GHz) increased with increasing loading of graphene for both solid and foam specimens, which is in good agreement with their electrical conductivities [45, 46]. As shown in Figure 5 a and a', with the same rGO loading, a higher SE value can be found in foamed specimens compared with solid specimens due to their higher electrical conductivity (Figure 4h) alongside with

multilevel wave reflection [47-49]. Due to higher thickness of foams caused by foaming process, the SE_T of m-EP/rGO microcellular nanocomposites were higher than that of their solid counterparts, which was in agreement with reported results [17]. The existence of porous structures within the m-EP/rGO foamed nanocomposites provides cavities to facilitate the multi-reflection and scattering of EMWs, lengthening the waves path, increasing the number of times that waves interact with conductive nanofiller and consequent contributing to the attenuation of induced EMWs [44]. For example, m-EP/rGO-4.55 solid presents EMI SE of 25.6 dB, lower than that of counterpart foam of 27.4 dB. At high rGO loading of 32.26 wt.%, a SE_T value of 83.5 dB is obtained for the solid specimen while a higher value of 86.6 dB for the foamed specimen.

Figure 5a" compares the total SE (SE_T), composed of reflected SE (SE_R) and absorbed SE (SE_A), and the specific total SE (SSE_T, SE_T divided by material density) of both solids and foams and shows that with the increased amount of conductive nanofillers, a clear increasing trend of SE_T, SE_R, SE_A and SSE_T can be observed for all m-EP/rGO solids and foams. The dominated SE_A indicated that shielding mechanism was mainly based on EMI absorption rather than reflection (Figure S22). Higher SSE_T is achieved in foams than in solids because of low density of foamed samples. The obtained EMI SE properties not only outperformed most absolute total SE of the nanocomposites with similar filler contents (Figure 5c), but also achieved a significantly improved specific total SE values (SSE_T) of 156.0 dB/(g/cm^3) from microcellular m-EP/rGO-32.26 specimen which is the highest value compared with any reported values from graphene reinforced epoxy nanocomposites in the literatures (Figure 5c inset). The practical tests illustrated in Figures S23 and video S1 are employed to evaluate the shielding efficiency of m-EP/rGO-32.26 foam and present the validity and reliability of the shielding materials on EMWs shielding capacity. Compared with m-EP/rGO-32.26 solid, the foamed one is lightweight and porous (Figure 1e and f), highly conductive (Figure 4h) and more excellent in EMI SE (Figure 5a' and a"), representing its potential as advanced shielding materials.

The shielding mechanism of current system is schematic illustrated in Figure 5b, with the incident waves striking onto the surface of materials and being partially reflected due to impedance mismatch - the difference in electromagnetic performance between shielding materials and ambient air [18, 50]. Then most of the EMWs in the nanocomposites are absorbed by highly conductive nanofillers because of the ohmic and dielectric loss, in which the well-dispersed and highly loaded rGO inside of current shielding materials can provide an efficient path to carry free

charges and forming eddy currents, that can transform electromagnetic energy into other type of energy (e.g. thermal energy). Meanwhile the rGO/m-EP interface can generate interfacial polarization, which benefits the dissipation of EMWs [51-54].

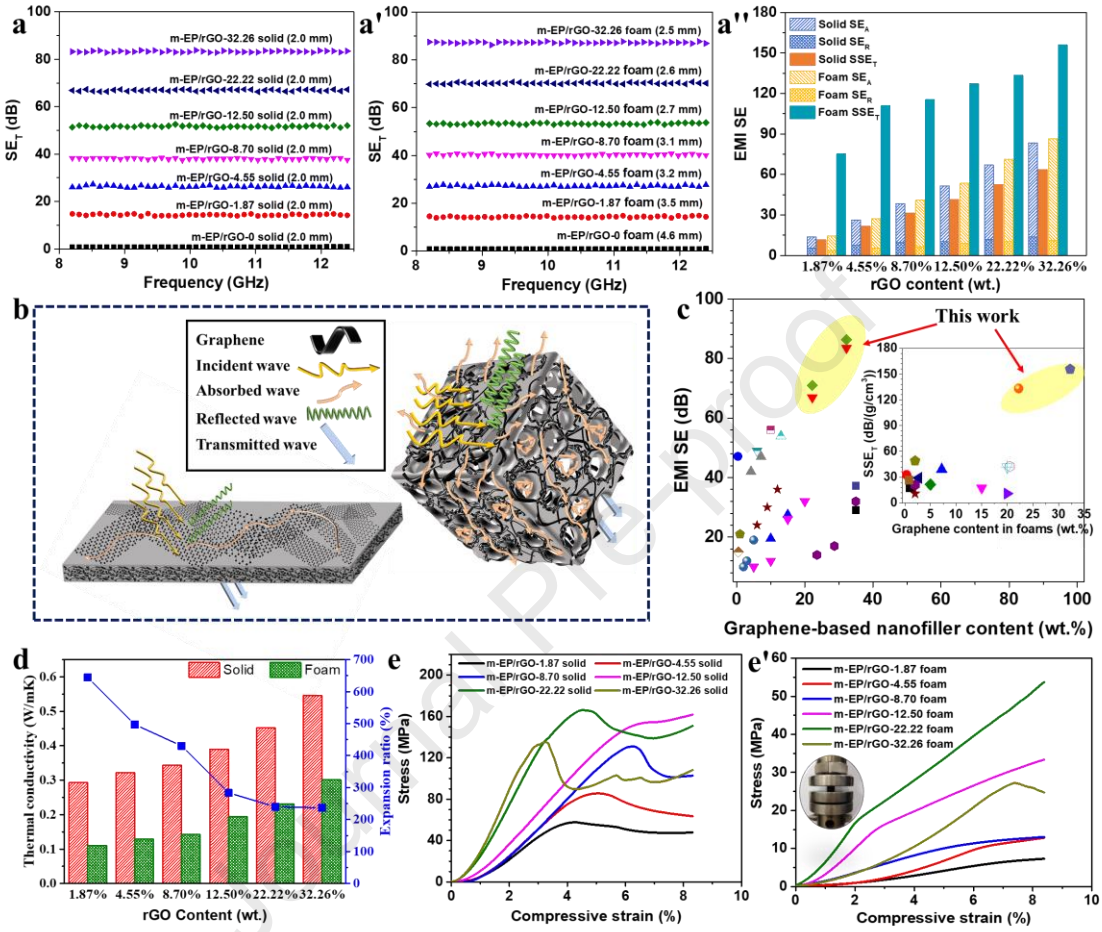

Figure 5 The electromagnetic interference (EMI) shielding effectiveness (SE) and thermal and mechanical performance of m-EP/rGO nanocomposites: EMI SE of m-EP/rGO solids (a) and foams (a') at X-band as well as (a'') individual contribution from absorbed SE (SE_A), reflected SE (SE_R) and specific total SE (SSE_T); (b) schematic illustrations of shielding mechanisms with EMWs reflection and attenuation in solid and foamed specimens; (c) comparison of EMI performance with literature values, showing the highest reported value from current m-EP/rGO nanocomposites; (d) thermal conductivity and volume expansion ratios of m-EP/rGO solids and foams; (e and e') mechanical properties of nanocomposites showing preserved compressive strength of foams at high nanofiller loadings due to well controlled microcellular structures

The thermal conductivity of both solid and foamed nanocomposites is presented in Figure 5d, showing an increasing trend with increased rGO loadings. The highest value of thermal conductivity of 0.50 W/mK was obtained from solid m-EP/rGO-32.26 specimen compared with other specimens in this work, while the lowest value of 0.12 W/mk was achieved in m-EP/rGO foam with 1.87 wt.% rGO content, attributing to the excellent thermal properties of graphene network with homogeneous dispersion. As the expansion ratio increased from foaming process, the thermal conductivity of foamed specimens was reduced compared to that of solid specimens, due to the increased cavities caused by porous structure [19, 55]. This inverse relationship between thermal conductivity and expansion ratio also can be seen from the lowest thermal conductivity correlated with the highest expansion ratio for the case of m-EP/rGO-1.87 foam. The thermal infrared measurements were also employed to examine the fabricated specimens (Figure S24), with the results in good agreement with their thermal conductivity values.

It is well acknowledged that the most graphene aerogels and its foams suffer from high brittleness with limited mechanical properties, i.e. compressive strength of only 8.0 kPa of pure aerogels (Figure S25), inevitably limiting their wider range of practical applications [23, 56-58]. The mechanical properties of fabricated m-EP/rGO nanocomposites were successfully preserved (Figure 5e), with compressive strength of 27.38 MPa at rGO loading over 30 wt.% alongside with a density as low as 0.55 g/cm^3. In the compressive stress-strain curves, continuous increase of stress in elastic region with rGO loading can be found in solids [59]. The compressive stress was increased with strain during the elastic region, then reached to the maximum yield strength and then reduced as the increment of strain. The trend of raised yield strength of the different m-EP/rGO solid nanocomposites could be found when the rGO loading ranged from 1.87 to 22.22 wt.% rGO. With the filler loading increased to be 32.26 wt.% loading, the compressive strength decreased due to the weaken interaction of rGO and m-EP matrix at high loading. However, owing to the existence of microporous structure after foaming processes, mechanical performance of a series of m-EP/rGO foams is lower than that of counterpart solids. To the best knowledge of authors, this mechanical property, especially at such high graphene loading level, is an outstanding reported value for foamed nanocomposites. (Table S4). Clearly, the well-preserved mechanical properties together with low density of microcellular m-EP/rGO nanocomposite could be utilized in many applications such as portable electronics and healthcare devices.

4. Conclusion

A novel strategy to fabricate epoxy/graphene nanocomposites with combined features of low density, outstanding electrical conductivity, high EMI properties, thermal insulation and mechanical strength, has been developed. The long-lasting dichotomy of dispersion and high loading of nanofillers in epoxy resins has been successfully overcome by infiltration m-EP into GA and tailoring the microcellular structures, with more than 30 wt.% of rGO well-dispersed in m-EP foam structures. Tailored modification of epoxy resins based on hyperbranched epoxy and plasticizers was employed to enable the successful $scCO_2$ foaming process after crosslinking of thermoset resins, hence to fabricate the nanocomposite microcellular foams from cured nanocomposites.

A synergistic effect between high loading of rGO and foaming process was found in this work, leading to a well-controlled cell morphology with enhanced electrical conductivity and cell wall strength. It is also worth noting that a balance between optimized porous structure and materials mechanical properties should be achieved, in order to promote both the thermal energy dissipation along the solid cell walls as well as the reflection and attenuation of EMWs within the cavities. Excellent electrical properties with conductivity of 3.14×10^2 S/m and EMI properties with specific total SE values of 156.3 dB/(g/cm^3) were achieved, which are among the highest reported values for graphene reinforced nanocomposites. The low density of only 0.55 g/cm^3 together with preserved mechanical properties of 27.4 MPa in compressive strength have demonstrated the feasibility of utilizing conductive polymer composites for next generation EMI shielding applications, such as portable electronics and devices where both high EMI SE as well as lightweight and structural properties are required.

Supporting Information.

Supplementary data to this article can be found online.

Declaration of Competing Interest

The authors declare that they have no known competing financial interests or personal relationships that could have appeared to influence the work reported in this paper.

Acknowledgements

The authors are grateful to the National Natural Science Foundation of China (Grant No.51773170) and Shaanxi Coal Joint Fund (Grant 2019JLM-24). This work is funded by the International Science &Technology Cooperation Plan of Shaanxi Province (2021KW-52), Fund of Natural Science Foundation of Shaanxi Provincial (2021JQ-111) and Fund of Basic and Applied Fundamental Research of Guangdong Provincial (2020A1515110861). The work is sponsored by Innovation Foundation for Doctor Dissertation of Northwestern Polytechnical University (No.CX202051). We would like to thank the Analytical & Testing Center of Northwestern Polytechnical University for equipment supporting.

References

[1] C. Vallés, X. Zhang, J. Cao, F. Lin, R.J. Young, A. Lombardo, A.C. Ferrari, L. Burk, R. Mülhaupt, I.A. Kinloch, Graphene/Polyelectrolyte Layer-by-Layer Coatings or Electromagnetic Interference Shielding, Appl. Nano Mater. 2 (2019) 5271-5281.

[2] J.M. Thomassin, C. Jerome, T. Pardoen, C. Bailly, I. Huynen, C. Detrembleur, Polymer/carbon-based composites as electromagnetic interference (EMI) shielding materials, Mat. Sci. Eng. R. 74 (2013) 211–232.

[3] W. Chen, W. Duan, Y. Liu, Q. Wang, F. Qi. Facile Fabrication of Multifunctional Polymer Composites Based on Three-Dimensional Interconnected Networks of Graphene and Carbon Nanotubes, Ind. Eng. Chem. Res. 58 (2019) 21531-21541.

[4] Z. Ma, S. Kang, J. Ma, L. Shao, Y. Zhang, C. Liu, A. Wei, X. Xiang, L. Wei, J. Gu. Ultraflexible and mechanically strong double-layered aramid nanofiber-Ti_3C_2Tx MXene/silver nanowire nanocomposite papers for high-performance electromagnetic interference shielding, ACS Nano 14 (2020) 8368-8382.

[5] Q. Song, F. Ye, L. Kong, Q. Shen, L. Han, L. Feng, G. Yu, Y. Pan, H. Li. Graphene and MXene Nanomaterials: Toward High-Performance Electromagnetic Wave Absorption in Gigahertz Band Range, Adv. Funct. Mater. 30 (2020) 2000475.

[6] C.W. Chu, J. Quyang, J.H. Tsen, Y. Yang. Organic Donor-Acceptor System Exhibiting Electrical Bistability for Use in Memory Devices, Adv. Mater. 17 (2005) 1440-1443.

[7] C. Xiang, Y. Pan, X. Liu, X. Sun, X. Shi, J. Guo, Microwave attenuation of multiwalled carbon nanotube-fused silica composites, Appl. Phys. Lett 87 (2005) 123103.

[8] Z. Ma, S. Kang, J. Ma, L. Shao, A. Wei, C. Liang, J. Gu, B. Yang, D. Dong, L. Wei, Z. Ji.

High-Performance and Rapid-Response Electrical Heaters Based on Ultraflexible, Heat-Resistant, and Mechanically Strong Aramid Nanofiber/Ag Nanowire Nanocomposite Papers, ACS Nano 12 (2019) 7578-7590.

[9] J. Liang, Y. Wang, Y. Huang, Y. Ma, Z. Liu, J. Cai, C. Zhang, H. Gao, Y. Chen. Electromagnetic interference shielding of graphene/epoxy composites, Carbon 47 (2009) 922–925.

[10] J. Ling, W. Zhai, W. Feng, B. Shen, J. Zhang, W. Zheng, Facile Preparation of Lightweight Microcellular Polyetherimide/Graphene Composite Foams for Electromagnetic Interference Shielding, ACS Appl. Mater. Interfaces 5 (2013) 2677−2684.

[11] J. Joseph, A.K. Koroth, D.A. John, A.M. Sidpara, J. Paul. Highly filled multilayer thermoplastic/graphene conducting composite structures with high strength and thermal stability for electromagnetic interference shielding applications, J. Appl. Polym. Sci. 136 (2019) 47792.

[12] Z. Ma, A. Wei, Y. Li, L. Shao, H. Zhang, X. Xiang, J. Wang, Q. Ren, S. Kang, D. Dong, J. Ma, G. Zhang, Lightweight, flexible and highly sensitive segregated microcellular nanocomposite piezoresistive sensors for human motion detection, Compos. Sci. Technol. 203 (2021) 108571.

[13] Z. Chen, C. Xu, C. Ma, W. Ren, H.M. Cheng. Lightweight and Flexible Graphene Foam Composites for High-Performance Electromagnetic Interference Shielding, Adv. Mater. 25 (2013) 1296–1300.

[14] Y. Chen, H.B. Zhang, Y. Yang, M. Wang, A. Cao, Z.Z. Yu, High-Performance Epoxy Nanocomposites Reinforced with Three-Dimensional Carbon Nanotube Sponge for Electromagnetic Interference Shielding. Adv. Funct. Mater. 26 (2016) 447–455.

[15] Y. Huangfu, C. Liang, Y. Han, H. Qiu, P. Song, L. Wang, J. Kong, J. Gu. Fabrication and investigation on the Fe_3O_4/thermally annealed graphene aerogel/epoxy electromagnetic interference shielding nanocomposites. Compos. Sci. Technol. 169 (2019) 70–75.

[16] D.X. Yan, H. Pang, B. Li, R. Vajtai, L. Xu, P.G. Ren, J.H. Wang, Z.M. Li. Structured Reduced Graphene Oxide/Polymer Composites for Ultra-Effi cient Electromagnetic Interference Shielding Adv. Funct. Mater. 25 (2015) 559–566.

[17] J. Liu, H.B. Zhang, R. Sun, Y. Liu, Z. Liu, A. Zhou, Z.Z. Yu, Hydrophobic, Flexible, and Lightweight MXene Foams for High-Performance Electromagnetic-Interference Shielding. Adv. Mater. 29 (2017) 1702367.

[18] H.B. Zhang, Q. Yan, W.G. Zheng, Z. He, Z.Z. Yu. Tough Graphene-Polymer Microcellular

Foams for Electromagnetic Interference Shielding. ACS Appl. Mater. Interfaces 3 (2011) 918–924.

[19] M. Hamidinejad, B. Zhao, A. Zandieh, N. Moghimian, T. Filleter, C.B. Park. Enhanced Electrical and Electromagnetic Interference Shielding Properties of Polymer−Graphene Nanoplatelet Composites Fabricated via Supercritical-Fluid Treatment and Physical Foaming. ACS Appl. Mater. Interfaces 10 (2018) 30752−30761.

[20] B. Shen, Y. Li, W. Zhai, W. Zheng. Compressible Graphene-Coated Polymer Foams with Ultralow Density for Adjustable Electromagnetic Interference (EMI) Shielding. ACS Appl. Mater. Interfaces 8 (2016) 8050−8057.

[21] M. Xu, H. Yan, Q. He, C. Wan, T. Liu, L. Zhao, C.B. Park, Chain extension of polyamide 6 using multifunctional chain extenders and reactive extrusion for melt foaming, European Polymer Journal 96 (2017) 210–220.

[22] P.T. Dirlam, D.J. Goldfeld, D.C. Dykes, M.A. Hillmyer, Polylactide Foams with Tunable Mechanical Properties and Wettability using a Star Polymer Architecture and a Mixture of Surfactants, ACS Sustainable Chem. Eng. 7 (2019) 1698–1706.

[23] H. Yang, Z. Li, G. Sun, X. Jin, B. Lu, P. Zhang, T. Lin, L. Qu. Superplastic Air-Dryable Graphene Hydrogels for Wet-Press Assembly of Ultrastrong Superelastic Aerogels with Infinite Macroscale. Adv. Funct. Mater. 29 (2019) 1901917.

[24] S. Wan, L. Jiang, Q. Cheng, Design Principles of High-Performance Graphene Films: Interfaces and Alignment, Matter 3 (2020) 696–707.

[25] P.G. Ren, D.X. Yan, X. Ji, T. Chen, Z.M. Li, Temperature dependence of graphene oxide reduced by hydrazine hydrate, Nanotechnology 22 (2011) 055705.

[26] S. Stankovich, D.A. Dikin, R.D. Piner, K.A. Kohlhaas, A. Kleinhammes, Y. Jia, Y. Wu, S. T. Nguyen, R.S. Ruoff, Synthesis of graphene-based nanosheets via chemical reduction of exfoliated graphite oxide, Carbon 45 (2007) 1558–1565.

[27] N. Yousefi, X. Lin, Q. Zheng, X. Shen, J.R. Pothnis, J.Jia, E. Zussman, J.K. Kim, Simultaneous in situ reduction, self-alignment and covalent bonding in graphene oxide/epoxy composites, Carbon. 59 (2013) 406-417.

[28] C. Bao, Y. Guo, L. Song, Y. Hu, Poly(vinyl alcohol) nanocomposites based on graphene and graphite oxide: a comparative investigation of property and mechanism, J. Mater. Chem. 21 (2011) 13942–13950.

[29] V.C. Tung, J. Kim, L.J. Cote, J. Huang, Sticky Interconnect for Solution-Processed Tandem Solar Cells. J Am Chem Soc. 133 (2011) 9262–9265.

[30] H. Yang, Z. Li, B. Lu, J. Gao, X. Jin, G. Sun, G. Zhang, P. Zhang, L. Qu. Reconstruction of Inherent Graphene Oxide Liquid Crystals for Large-Scale Fabrication of Structure-Intact Graphene Aerogel Bulk toward Practical Applications, ACS Nano 12 (2018) 11407-11416.

[31] S. Gupta, N.H. Tai. Carbon materials and their composites for electromagnetic interference shielding effectiveness in X-band, Carbon 152 (2019) 159-187.

[32] A. Ito, T. Semba, K. Taki, M. Ohshima, Effect of the Molecular Weight between Crosslinks of Thermally Cured Epoxy Resins on the CO_2-Bubble Nucleation in a Batch Physical Foaming Process, J. Appl. Polym. (2014) 40407 1-8.

[33] S.A. Syed Asif, K.J. Wahl, R.J. Colton, Nanoindentation and contact stiffness measurement using force modulation with a capacitive load-displacement transducer. Rev. Sci. Instrum. 70 (1999) 2408-2413.

[34] A. Saikia, D. Hazarika, N. Karak, Tough and biodegradable thermosets derived by blending of renewable resource based hyperbranched epoxy and hyperbranched polyester, Polymer Degradation and Stability 159 (2019) 15-22.

[35] K.Y. Andrew Lin, A.H. Alissa Park, Effects of bonding types and functional groups on CO_2 capture using novel multiphase systems of liquid-like nanoparticle organic hybrid materials, Environ. Sci. Technol. 45 (2011) 6633-6639.

[36] X. Fan, G. Zhang, J. Li, Z. Shang, H. Zhang, Q. Gao, J. Qin, X. Shi, Study on foamability and electromagnetic interference shielding effectiveness of supercritical CO_2 foaming epoxy/rubber/MWCNTs composite. Compos. Part A-Appl S, 121 (2019) 64-73.

[37] A. Chakravartula, K. Komvopoulos. Viscoelastic properties of polymer surfaces investigated by nanoscale dynamic mechanical analysis, Appl. Phys. Lett. 88 (2006) 131901.

[38] J. Li, G. Zhang, H. Zhang, X. Fan, L. Zhou, Z. Shang, X. Shi, Electrical conductivity and electromagnetic interference shielding of epoxy nanocomposite foams containing functionalized multi-wall carbon nanotubes, Applied Surface Science 428 (2018) 7–16.

[39] Q. Gao, G. Zhang, X. Fan, H. Zhang, Y. Zhang, F. Huang, R. Xiao, X. Shi, J. Qin, Enhancements of foamability, electromagnetic interference shielding and mechanical property of epoxy microcellular composite foam with well dispersed f-MWCNTs, Composites Part A 138 (2020) 106060.

[40] S. Liu, R. Eijkelenkamp, J. Duvigneau, G.J. Vancso, Silica-Assisted Nucleation of Polymer Foam Cells with Nanoscopic Dimensions: Impact of Particle Size, Line Tension, and Surface Functionality, ACS Appl. Mater. Inter. 9 (2017) 37929-37940.

[41] Q. Peng, Y. Li, X. He, X. Gui, Y. Shang, C. Wang, C. Wang, W. Zhao, S. Du, E. Shi, P. Li, D. Wu, A. Cao. Graphene Nanoribbon Aerogels Unzipped from Carbon Nanotube Sponges. Adv. Mater. 26 (2014) 3241–3247.

[42] X.H. Li, X. Li, K.N. Liao, P. Min, T. Liu, A. Dasari, Z.Z. Yu. Thermally Annealed Anisotropic Graphene Aerogels and Their Electrically Conductive Epoxy Composites with Excellent Electromagnetic Interference Shielding Efficiencies. ACS Appl. Mater. Interfaces 8 (2016) 33230−33239.

[43] J. Li, Y. Ding, N. Yu, Q. Gao, X. Fan, X. Wei, G. Zhang, Z. Ma, X. He, Lightweight and stiff carbon foams derived from rigid thermosetting polyimide foam with superior electromagnetic interference shielding performance, Carbon 158 (2020) 45-54.

[44] F. Shahzad, M. Alhabeb, C.B. Hatter, B. Anasori, S.M. Hong, C.M. Koo, Y. Gogotsi. Electromagnetic interference shielding with 2D transition metal carbides. Science 353 (2016) 1136-1140.

[45] S. Liu, S. Yin, J. Duvigneau, G.J. Vancso, Bubble Seeding Nanocavities: Multiple Polymer Foam Cell Nucleation by Polydimethylsiloxane-Grafted Designer Silica Nanoparticles, ACS Nano 14 (2020) 1623−1634.

[46] J. Li, G. Zhang, X. Fan, X. Fan, L. Zhou, J. Li, X. Shi, H. Zhang, Preparation and mechanical properties of thermosetting epoxy foams based on epoxy/2-ethyl-4-methylimidazol system with different curing agent contents, J. Cell. Plast, 53 (2017) 663-681.

[47] M. Soltani Alkuh, M.H.N. Famili, M. Mokhtari Motameni Shirvan, M.H. Moeini, The relationship between electromagnetic absorption properties and cell structure of poly(methyl methacrylate)/multi-walled carbon nanotube composite foams. Mater. Design 100 (2016) 73-83.

[48] I. Huynen, N. Quie´vy, C. Bailly, P. Bollen, C. Detrembleur, S. Eggermont, I. Molenberg, J. M. Thomassin, L. Urbanczyk, T. Pardoen, Multifunctional hybrids for electromagnetic absorption, Acta Mater 59 (2011) 3255–3266.

[49] J. Chen, X. Liao, W. Xiao, J. Yang, Q. Jiang, G. Li, Facile and Green Method To Structure Ultralow-Threshold and Lightweight Polystyrene/MWCNT Composites with Segregated

Conductive Networks for Efficient Electromagnetic Interference Shielding, ACS Sustainable Chem. Eng. 7 (2019) 9904–9915.

[50] J. Li, Y. Ding, Q. Gao, H. Zhang, X. He, Z. Ma, B. Wang, G. Zhang, Ultrathin and flexible biomass-derived C@CoFe nanocomposite films for efficient electromagnetic interference shielding, Composites Part B-Engineering, 190 (2020) 107935.

[51] G. Gedler, M. Antunes, J.I. Velascoa, R. Ozisikb. Enhanced electromagnetic interference shielding effectiveness of polycarbonate/graphene nanocomposites foamed via 1-step supercritical carbon dioxide process. Mater. Design 90 (2016) 906-914.

[52] B. Shen, Y. Li, D. Yi, W. Zhai, X. Wei, W. Zheng, Microcellular graphene foam for improved broadband electromagnetic interference shielding, Carbon 120 (2016) 154-160.

[53] H. Zhang, G. Zhang, M. Tang, L. Zhou, J. Li, X.Fan, X. Shi, J. Qin, Synergistic effect of carbon nanotube and graphene nanoplates on the mechanical, electrical and electromagnetic interference shielding properties of polymer composites and polymer composite foams, Chem. Eng. J. 353 (2018) 381-393.

[54] S. Kang, H. Choi, S. B.Lee, S.C. Park, J. B. Park, S. Lee, Y. Kim, B.H. Hong, Efficient heat generation in large-area graphene films by electromagnetic wave absorption, 2D Mater. 4 (2017) 02503.

[55] Q. Song, F. Ye, X. Yin, W. Li, H. Li, Y. Liu, K. Li, K. Xie, X. Li, Q. Fu, L. Cheng, L. Zhang, B. Wei. Carbon Nanotube–Multilayered Graphene Edge Plane Core–Shell Hybrid Foams for Ultrahigh-Performance Electromagnetic-Interference Shielding, Adv. Mater. 29 (2017) 1701583.

[56] M. Wang, X. Duan, Y. Xu, X. Duan. Functional Three-Dimensional Graphene/Polymer Composites. ACS Nano 10 (2016) 7231−7247.

[57] X. Fan, G. Zhang, Q. Gao, J. Li, Z. Shang, H. Zhang, Y. Zhang, X. Shi, J. Qin, Highly expansive, thermally insulating epoxy/Ag nanosheet composite foam depending on supercritical CO_2 for interference shielding performance. Chem. Eng. J. 372 (2019) 191-202.

[58] J. Zhao, Q. Zhao, C. Wang, B. Guo, C.B. Park, G. Wang, High thermal insulation and compressive strength polypropylene foams fabricated by high-pressure foam injection molding and mold opening of nano-fibrillar composites. Mater. Des. 131 (2017) 1–11.

[59] X. Han, T. Wang, P.S.Owuor, S. H. Hwang, C. Wang, J. Sha, L. Shen, J. Yoon, W. Wang, R. V. Salvatierra, P. M. Ajayan, R.Shahsavari, J. Lou, Y. Zhao, J. M. Tour, Ultra-Stiff Graphene Foams as Three-Dimensional Conductive Fillers for Epoxy Resin. ACS Nano 12 (2018) 11219-

11228

Highlights

1. A strategy to prepare m-EP/rGO nanocomposite with 32.26 wt.% rGO loading and uniform dispersion

2. Controlled foamability of thermosetting nanocomposites by $scCO_2$ foaming process

3. Excellent electrical conductivity (3.14×10^2 S/m) and EMI SE (SE_T=86.6 dB) achieved from m-EP/rGO foam

Declaration of interests

☒ The authors declare that they have no known competing financial interests or personal relationships that could have appeared to influence the work reported in this paper.

☐The authors declare the following financial interests/personal relationships which may be considered as potential competing interests: